Size-induced sign inversion of line tension in nanobubbles at a solid/liquid interface

Naoki Kameda, Seiichiro Nakabayashi *

Department of Chemistry, Faculty of Science, Saitama University, Saitama 338-8570, Japan

Received 10 October 2007; in final form 23 June 2008

Abstract

Small bubbles with average diameters of 10 and 100 nm were spontaneously formed on the surface of Au(111) in contact with air-saturated water and ethanol-water 1/4 solution, respectively. Analyses of topographic images of the bubbles demonstrated that the contact line tension changed sign, from negative to positive, with a decrease in the bubble size. Despite the apparent stability and long lifetime of the bubbles, both of these bubble systems were found to be thermodynamically unstable, as estimated from the free energies of bubble formation by combination of their surface and line energies.

* Corresponding author.
E-mail address: Sei@chem.saitama-u.ac.jp (S.Nakabayashi).

Kameda

Graphical Abstract

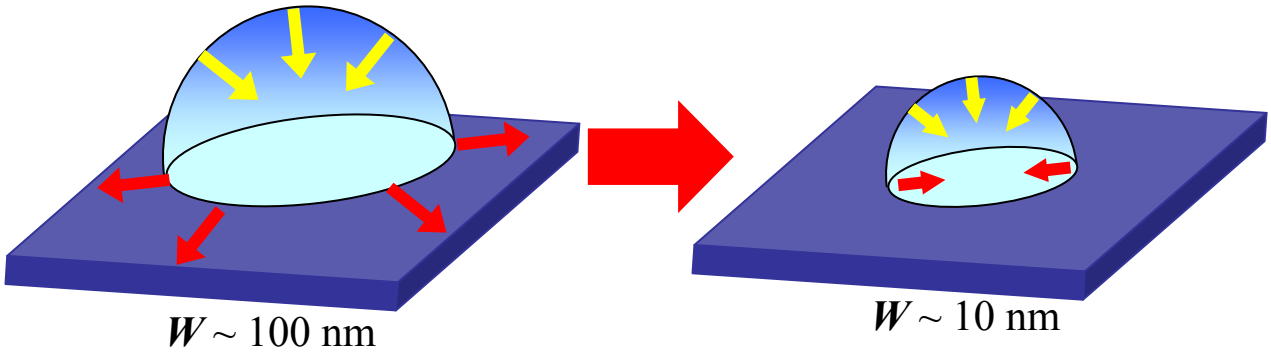

1. Introduction

Nanometer-sized bubbles appearing on hydrophobic solid surfaces in contact with gas containing aqueous solutions [1-5] are one of the promising fields of spontaneously assembled nanostructures in confined geometries. Surface-sensitive hydrodynamics have revealed no-zero lateral velocities at interfaces [6], although standard boundary conditions for the fluid flow along the solid wall is a non-slip condition. An analysis of the motions of spin-probe molecules has confirmed that a liquid can flow through the nano-pores of MCM-41 [7], whose diameter is accurately tuned in the range of 2 – 25 nm [8].

These reports suggest the presence of nanobubbles at interfaces. Related phenomena at confined hydrophobic interfaces have been observed in various biological channel proteins penetrating through cell membranes, where stochastic liquid-vapor oscillations of confined water have been studied experimentally and theoretically [9-11].

In spite of such ubiquity, understanding of these behaviors of nanobubbles is still limited. One of the fundamental questions is their thermodynamic stability. Experimentally, these nanobubbles are stable over hours, although the lifetimes of those with radii of ~ 100 nm have been estimated to be shorter than 1 s due to the Laplace pressure, i. e., an additional internal pressure up to 10 atm caused by surface tension [12,13].

The stability of small bubbles and/or droplets on a solid surface is affected by the energy of the line on which the three phases meet [14-18]. The excess free energy per unit length of the line is the line tension, τ. For small enough bubbles, τ critically contributes to stabilization, but it is negligible for larger bubbles (> 10 μm in radius).

The present article reports on the thermodynamic stabilities in these systems. We have examined the contact line tension of nanobubbles at an atomically flat Au(111) surface by a size adjustment of the bubbles by addition of ethanol to water. Their topographical images have been analyzed by an atomic force microscope (AFM), from which the Gibbs energies of single bubble formation are estimated.

2. Experimental

Au(111) substrates were prepared by sputtering gold (99.99%, Tanaka-Kikinzoku) onto freshly cleaved mica (Ohken-Shoji). The thickness of the gold film was 200 nm.

The substrates were annealed at 773 K in vacuum to produce wide terraces on the Au(111) single crystal surface. A clean Au(111) surface in the ambient air is known to be highly sensitive to airborne hydrophobic contaminants. In these experiments, the contact angles of a sessile water drop, θ_Y, were $40^o < \theta_Y < 60^o$. Since the clean Au(111) surface is hydrophilic with $\theta_Y \sim 20^o$ [19,20], our surface was not perfectly contaminant-free. However, since θ_Y became ~ 80^o while the crystal was kept over 1 h in the ambient air, the cleanness of the used surface was the upper limit achieved under our experimental conditions.

The substrate was held in a fluidic cell of AFM, and the liquid surface was opened to the ambient air. Milli-Q water with conductivity less than 1×10^{-6} S cm^{-1} was used. Air had been bubbled into the water over 1 h before use to maintain air saturation. The ethanol/water ratio of the aqueous solution was 1/4 in volume. The AFM (Nanoscope III, Veeco) was operated under the tapping mode (TM). In order to suppress mechanical perturbation, an extra electronic circuit (Q-control; Nano-analytics) was added to increase the Q factor of the electromechanical system. The effective Q factors in air and in water were 3000 and 30, respectively.

3. Results

3.1. AFM images

TM-AFM images of Au(111) in air and the cross section are shown Fig. 1a. The flatness of the surface is within ± 0.2 nm along the 2.0 μm broken line. The step lines cross each other with 60°, which assures that the atomic arrangement on the substrate surface is well ordered [21]. As shown in Fig. 1b, small bubbles with widths W of ~ 10 nm are observed in the AFM image at the interface in contact with air-saturated water. In contrast, much larger bubbles, W ~ 100 nm, are observed in the corresponding image of ethanol/water, as shown in Fig. 1c. The heights h of the bubbles, 0.6 – 1.2 and 10 – 50 nm in Figs. 1b and c respectively, differ from each other by one order of magnitude. The histograms of h, W, and the radius of the truncated sphere, R, shown Fig. 2, are fitted to Gaussian functions after correction on the W and R values for a spherical cap by the following procedure.

3.2. Estimation of bubble radii

Since the radius of curvature of the AFM tip (R_{tip} ~ 15 nm) was comparable with those of the bubbles, the AFM images contained a geometric artifact. Under the assumption that the bubble shape is a truncated sphere (i.e., a spherical cap), as shown in Fig. 3a, the apparent width W' is overestimated since the tip contacts with the bubble at P' instead of P. Real R and W values can be estimated from R_{tip} and W' by

$$R = (1/2h)\{(W'/2)^2 + h^2\} - R_{tip} \qquad (1)$$

$$W = (2Rh - h^2)^{1/2} \qquad (2)$$

Equations (1) and (2) do not contain the vertical correction; the measured h can be regarded as reliable, because the jump-in distance in the force-separation curve is identical with the uncorrected h value. This consistency originates from the Q-control circuit that decreases the mechanical perturbation in the vertical direction. As shown in the force-separation curve in Fig. 4a, the contact of the needle with the bubble induces a sizable hysteresis between the jump-in and the jump-out by a viscoelastic deformation of the bubble. The jump-in distance is less than 3 nm. The consistency of h with the jump-in distance supports that no correction is needed for h.

The validity of the spherical cap assumption made in Eqs. (1) and (2) is examined by checking the deviations of the observed W/h and h values from those based on the ideal truncated spheres, shown in Figs. 4b and c as solid lines. The deviations are larger for smaller bubbles (open circles) than for larger bubbles (filled circles).

3.3. Estimation of bubble free energy

The surface area Γ, the circle of three-phase contact $A = \pi W^2/4$, and the Gibbs energy G for the formation of a spherical bubble are geometrically given by

$$\Gamma = 2\pi R^2(1 - \cos\theta) \qquad (3)$$

$$W = 2R \sin\theta \qquad (4)$$

$$G = \gamma_{LV}\Gamma + (\gamma_{SV} - \gamma_{SL})\pi(W/2)^2 + \pi W\tau_{SLV} \qquad (5)$$

where γ_{SV}, γ_{SL} and γ_{LV} are the surface free energies of solid-vapor, solid-liquid and liquid-vapor interfaces, respectively, and τ_{SLV} is the contact line energy on the boundary of solid-liquid-vapor phases [14] . The minimum Gibbs energy G of the spherical bubble, where $dG/d\theta = 0$, is estimated by [14]

$$\cos\theta = \cos\theta_Y - 2\tau_{SLV} / W\gamma_{LV} \qquad (6)$$

$$\cos\theta_Y = (\gamma_{SL} - \gamma_{SV})/\gamma_{LV} \quad (7)$$

where θ is the microscopic contact angle obtained by the TM-AFM image and extrapolation to the macroscopic Young contact angle θ_Y ($W\rightarrow\infty$). Equations (6) and (7) are called the modified Young (or Young-Dupré) and Young equations, respectively [14-18]. Equation (6) indicates that a smaller size of the bubble requires a higher energy contribution of the contact line.

The relationship between cos θ and $2/W$ is plotted in Fig. 5. Equation (6), which would lead to a straight line with a slope of $-\tau_{SLV}/\gamma_{LV}$, does not fit to the experimental plot in Fig. 5a. The plot for the larger bubbles in ethanol/water, shown in Fig. 5b, has a *positive* slope, $\tau_{SLV}/\gamma_{LV} = -0.77$ nm, whereas that in water has a *negative* slope, τ_{SLV}/γ_{LV} = 0.63 nm. The surface energies at the liquid and air interface, γ_{LV}, (i. e., the macroscopic surface tensions) are 2.8×10^{-2} and 7.2×10^{-2} J/m^2 for ethanol/water and water, respectively [22,23]. Hence, the line tensions τ_{SVL} are estimated to be -2×10^{-10} and 5×10^{-11} J/m, respectively. The negative line tension tends to expand the three-phase contact line and is expected to balance the surface tension that shrinks the bubble. In contrast, the positive line tension works with the surface tension that shrinks the bubble. These trends are in accord with the observed macroscopic contact angles θ_Y ($W\rightarrow\infty$) of 38 and 0^o for the air bubbles in ethanol/water and water, respectively.

4. Discussion

4.1. Possible candidate for additional stabilization

For the two kinds of nanobubbles, τ_{SVL}, cos θ_Y, the total surface energy E_S, the total line energy E_L and the formation Gibbs energy of a single bubble G are listed in Table 1. It is found that a smaller nanobubble ($W \sim 10$ nm) has positive line tension and requires 5.6×10^{-18} J for bubble formation, whereas a larger nanobubble ($W \sim 200$ nm) has a negative line tension and the formation energy of 1.4×10^{-16} J. Both of these bubbles are thermodynamically unstable, but they are experimentally in steady states, because these nanobubbles have lifetimes as long as several hours. This additional stabilization is probably supplied from the surface to the bubbles.

Electrostatic interaction between the bubbles and the Au(111) surface is one of the candidates, because a clean gold surface dipped in water is negatively charged (–1.4

mC/m^2) [24,25]. However, the TM-AFM images of the nanobubbles were found to be independent of the ionic concentration after addition of NaCl to 1×10^{-4} mol/l. This experimental finding suggests that electrostatic stabilization is negligible, because the screening of electrostatic interaction by the added ions should significantly modify the bubble shape. After all, no detail of this appreciable energy supply has yet been specified at the present stage.

4.2. Sign inversion of line tension

Another unexpected observation in Fig. 5 is the reversal of signs of the line tension with a decrease in W. It has been reported in this connection that cos θ for μm- to nm-sized alkane drops [16] depends nonlinearly on $(1/W)$ at constant room temperature and that the slope $(-\tau_{SLV}/\gamma_{LV})$ tends to zero with a decrease in the size. Inversion of the line tension from negative to positive has usually been observed at wetting transition temperature, T_w [14]; droplets appear on the surface at temperatures below T_w, but the three-phase contact line disappears above T_w. These features are consistent with the thermodynamic point of view. An increase in the number of drops with negative line tension ($T < T_w$) decreases the total energy of the wetting layer, but under positive line tension ($T > T_w$) the three-phase contact lines disappear and decrease the total energy.

As for the nanobubbles, the asymptotic contact angle θ_Y is zero in the plot of open circles in Fig. 5. This suggests that complete wetting by an air nanolayer is a stable state, but that smaller bubbles with positive line tension is probably a metastable state composed of torn pieces of complete wetting layers. For the larger bubbles in water/ethanol, the stable state is partially wetting by air nanolayers with $\theta_Y = 38^o$ and with negative line tension.

4.3. Limitation of the present discussion

The practical difficulty that prevents our further discussion is the uncontrollable chemical and topographical heterogeneity of the Au(111) surface used in the present experimental work. The surface roughness of Au(111) was ~ ± 0.2 nm in the height along the 2-μm horizontal line. For the bubbles in water, with W ~ 10 nm, the surface cannot be regarded as homogeneous because W exceeds the surface roughness by two

orders of magnitude, while h is in the same order. For the larger bubbles in the ethanol/water medium, on the other hand, the surface is effectively flat and homogeneous.

In spite of these uncontrollable surface factors at the present stage, the estimated line tensions, $\tau_{SLV} \sim -2\times10^{-10}$ and 5×10^{-11} J/m for the larger and smaller bubbles, respectively, are consistent with the reported general trend derived from a phenomenological log-log plot of the absolute values of the line tension covering ten orders of magnitude of variation in W, $10^{-9} \sim 10^{-2}$ m [18]. The line tensions estimated in our experiments are in line with the general trend, but the bubble formation energies by the combination of the surface and line energies cannot quantitatively explain the apparent stabilities of the larger and smaller bubbles.

5. Conclusion

Nanobubbles at Au(111) and aqueous liquid interface can be classified into two categories: larger bubbles, $W \sim 100$ nm, which have negative line tension in ethanol/water, and smaller bubbles, $W \sim 10$ nm, which have positive line tension in water. An additional stabilization by the surface is required in either case to account for this apparent stability, but the mechanism of the energy supplies is still to be explored in future studies.

Acknowledgements

Some of the Au(111) substrates used in this work were donated by Profs. H. Sakaguchi at Sizuoka University, I. Otsuka at Ohu University and S. Nagashima at Nihon University.

References

[1] N. Ishida, T. Inoue, M. Miyahara, K. Higashitani, Langmuir 16 (2000) 6377.

[2] J.W.G. Tyrrel, P. Attard, Phys. Rev. Lett. 87 (2001) 176104.

[3] D.A. Doshi, E.B. Watkins, J.N. Israelachvili, J. Majewski, Proc. Natl. Acad. Sci. U. S. A. 102 (2005) 9458.

[4] V. Tsionsky, A. Kaverin, L. Daikhin, G. Katz, E. Gileadi, Phys. Chem. Chem. Phys. 7 (2005) 1830.

[5] X.H. Zhang, A. Khan, W.A. Ducker, Phys. Rev. Lett. 98 (2007) 136101.

[6] P.G. de Gennes, Langmuir 18 (2002) 3413.

[7] C.T.Kresge, M/E/Leonowicz, W.J.Roth, J.C.Vartuli, J.S.Beck. Nature 359 (1992) 710.

[8] S. Anandan, M. Okazaki, Micropor. Mesopor. Mater. 87 (2005) 77.

[9] K. Lum, D. Chandler, J.D. Weeks, J. Phys. Chem. B 103 (1999) 4570.

[10] O. Beckstein, M.S.P. Sansom, Proc. Natl. Acad. Sci. U. S. A. 100 (2003) 7063.

[11] P. Pohl, S.M. Saparov, M.J. Borgnia, P. Agre, Proc. Natl. Acad. Sci. U. S. A. 98

[12] S. Ljunggren, J.C. Eriksson, Colloids Surf. A 129-130 (1997) 151.

[13] S. Yang, S.M. Dammer, N. Bremond, H.J.W. Zandvliet, E.S. Kooij, D. Lohse, Langmuir 23 (2007) 7072.

[14] B. Widom, J. Phys. Chem. 99 (1995) 2803.

[15] J.Y. Wang, S. Betelu, B.M. Law, Phys. Rev. E 63 (2001) 031601.

[16] A. Checco, P. Guenoun, J.Daillant, Phys. Rev. Lett. 91 (2003) 186101.

[17] J. Yang, J. Duan, D. Fornasiero, J. Ralston, J. Phys. Chem. B 107 (2003) 6139.

[18] R. David, A.W. Neumann, Langmuir 23 (2007) 11999.

[19] T. Smith, J. Colloid. Interface Sci. 75 (1980) 51.

[20] L. Chai, J. Klein, Langmuir 23 (2007) 7777.

[21] E. Holland-Moritz, J. Gordon II, G. Borges, R. Sonnenfeld, Langmuir 7 (1991) 301.

[22] The Chemical Society of Japan (Ed.), Kagaku Binran (Handbook of Chemistry), 5th ed. Tokyo, 2004, p. II-92.

[23] C.J. West, C. Hull, International Critical Tables of Numerical Data, Physics, Chemistry and Technology, McGraw-Hill, New York, 1993, p. 467.

[24] A. Chen, J. Lipkowski, J. Phys. Chem. B 103 (1999) 682.

[25] X.H. Zheng, N. Maeda, V.S.J. Craig, Langmuir 22 (2006) 5025.

Figure captions

Fig. 1. Typical topographic TM-AFM images of Au(111) in ambient air (a), in contact with water (b) and ethanol/water (1/4 in volume) solution (c). Plot below (a) is the cross section along the dotted line in the image.

Fig. 2. Histograms of the bubble (a) height, h, (b) width, W and (c) radius of curvature, R. The open and the filled rectangles are the bubbles in water and in ethanol/water, respectively.

Fig. 3. Schematic representation for (a) the bubble and (b) the correction of the topographic image of the bubble.

Fig. 4. Typical force-separation curve for the bubble in water (a). Plots of (W/h) against h in (b) tall and (c) short regions. Solid lines represent ideal spherical fitting curves with different radii of curvatures, R. Open and filled circles denote the bubbles in water and in ethanol/water.

Fig. 5. Young-Dupré plots for the bubbles in water (open circles) and ethanol/water (filled circles) in regions of (a) large and (b) small (2/W) values.

Kameda

Fig. 1

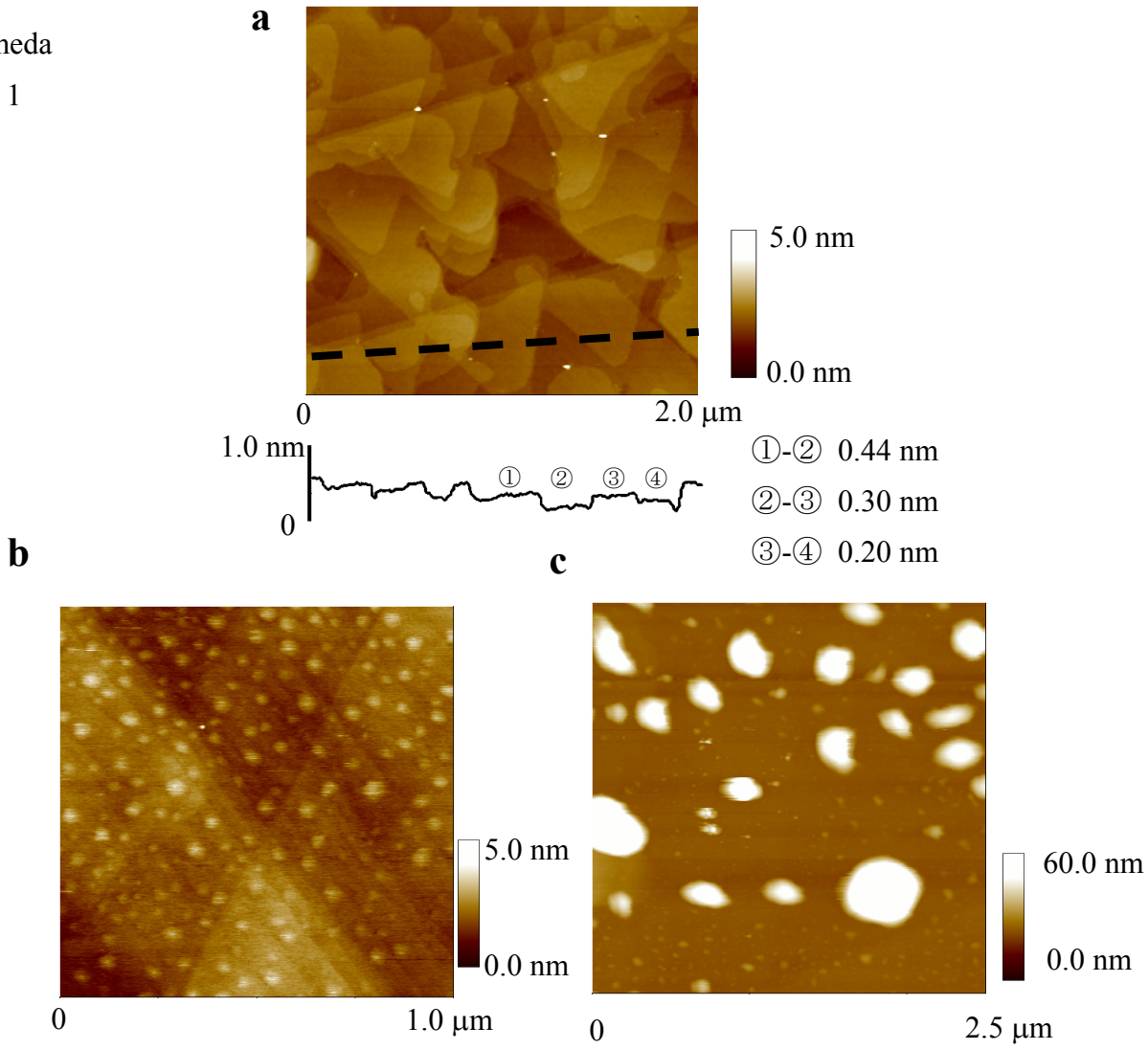
a
5.0 nm
0.0 nm
0
2.0 μm
1.0 nm
0
①
②
③
④
①-② 0.44 nm
②-③ 0.30 nm
③-④ 0.20 nm
b
5.0 nm
0.0 nm
0
1.0 μm
c
60.0 nm
0.0 nm
0
2.5 μm

Kameda

Fig. 2

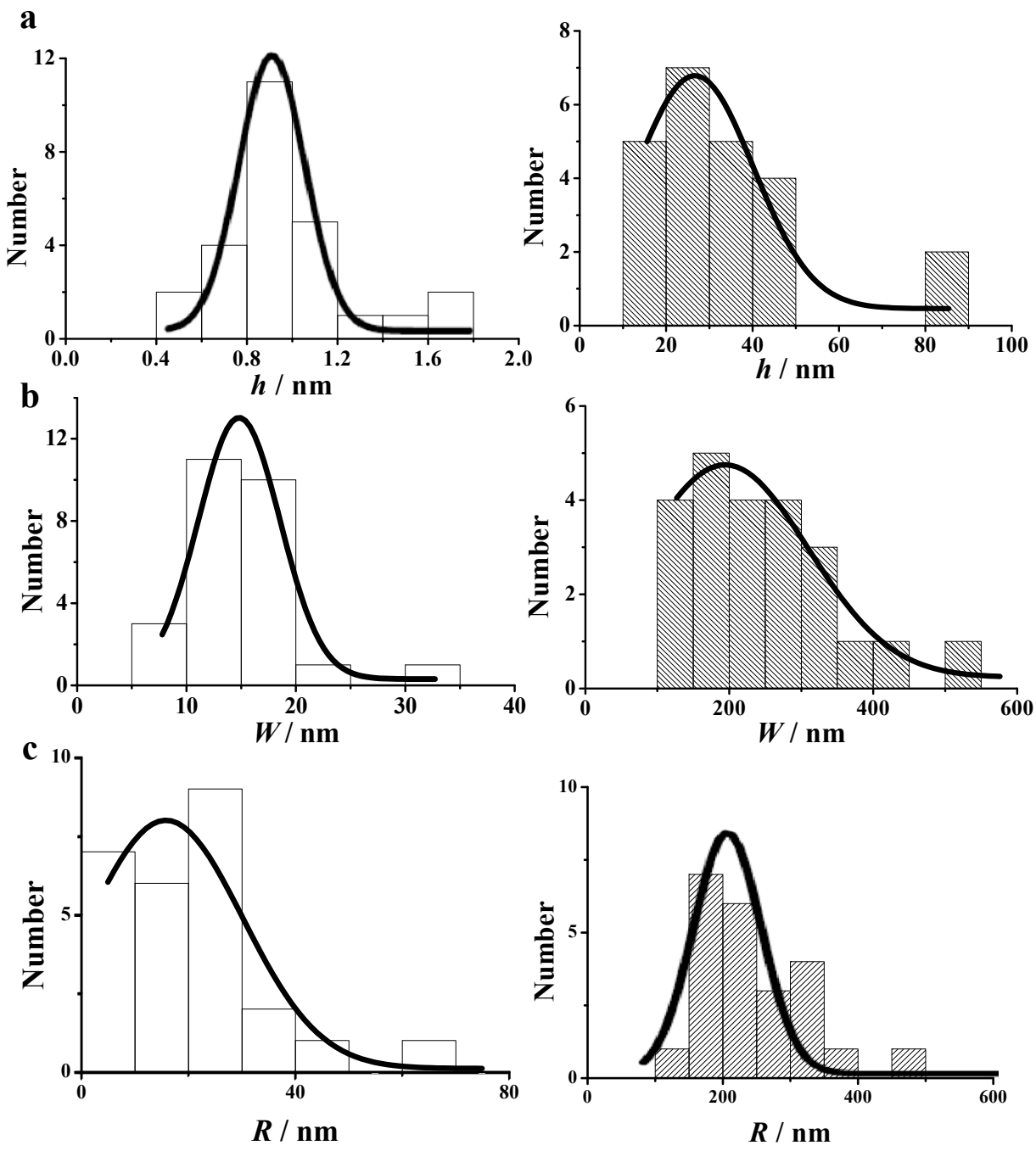

Kameda

Fig.3

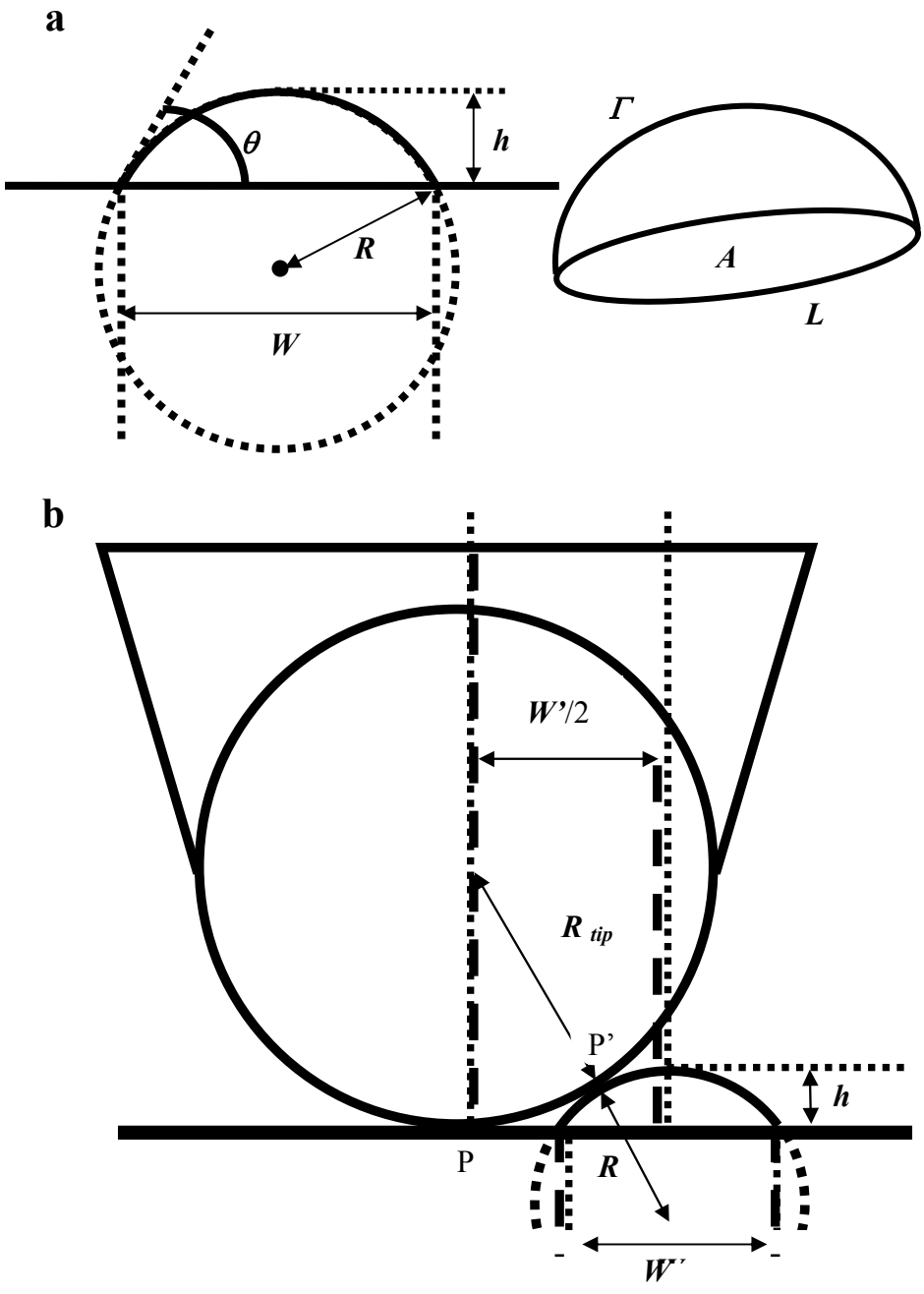

Kameda

Fig. 4

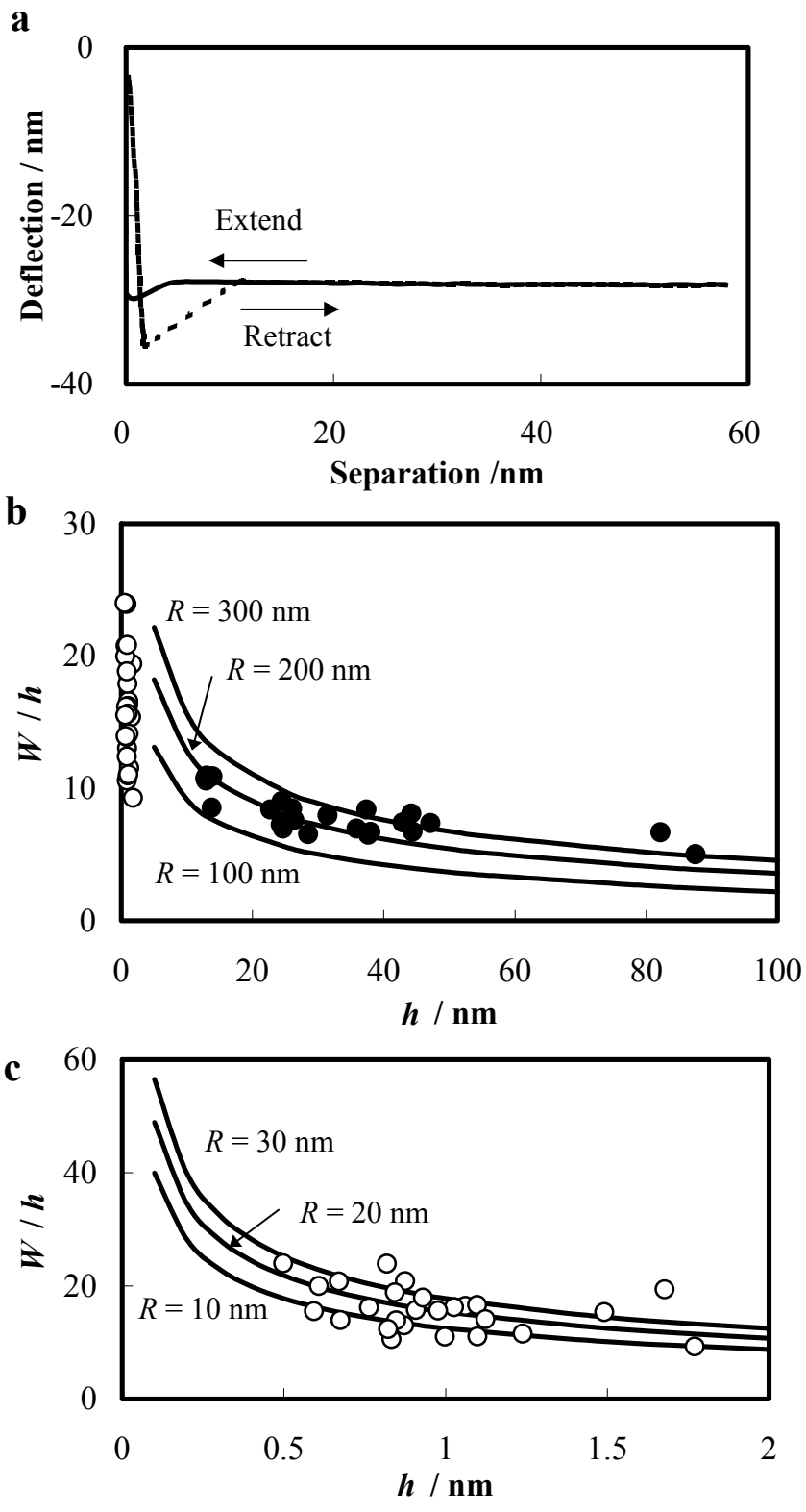
a
0
-20
-40
Deflection / nm
Extend
Retract
0
20
40
60
Separation /nm
b
30
20
10
0
W / h
R = 300 nm
R = 200 nm
R = 100 nm
0
20
40
60
80
100
h / nm
c
60
40
20
0
W / h
R = 30 nm
R = 20 nm
R = 10 nm
0
0.5
1
1.5
2
h / nm

Kameda Fig. 5

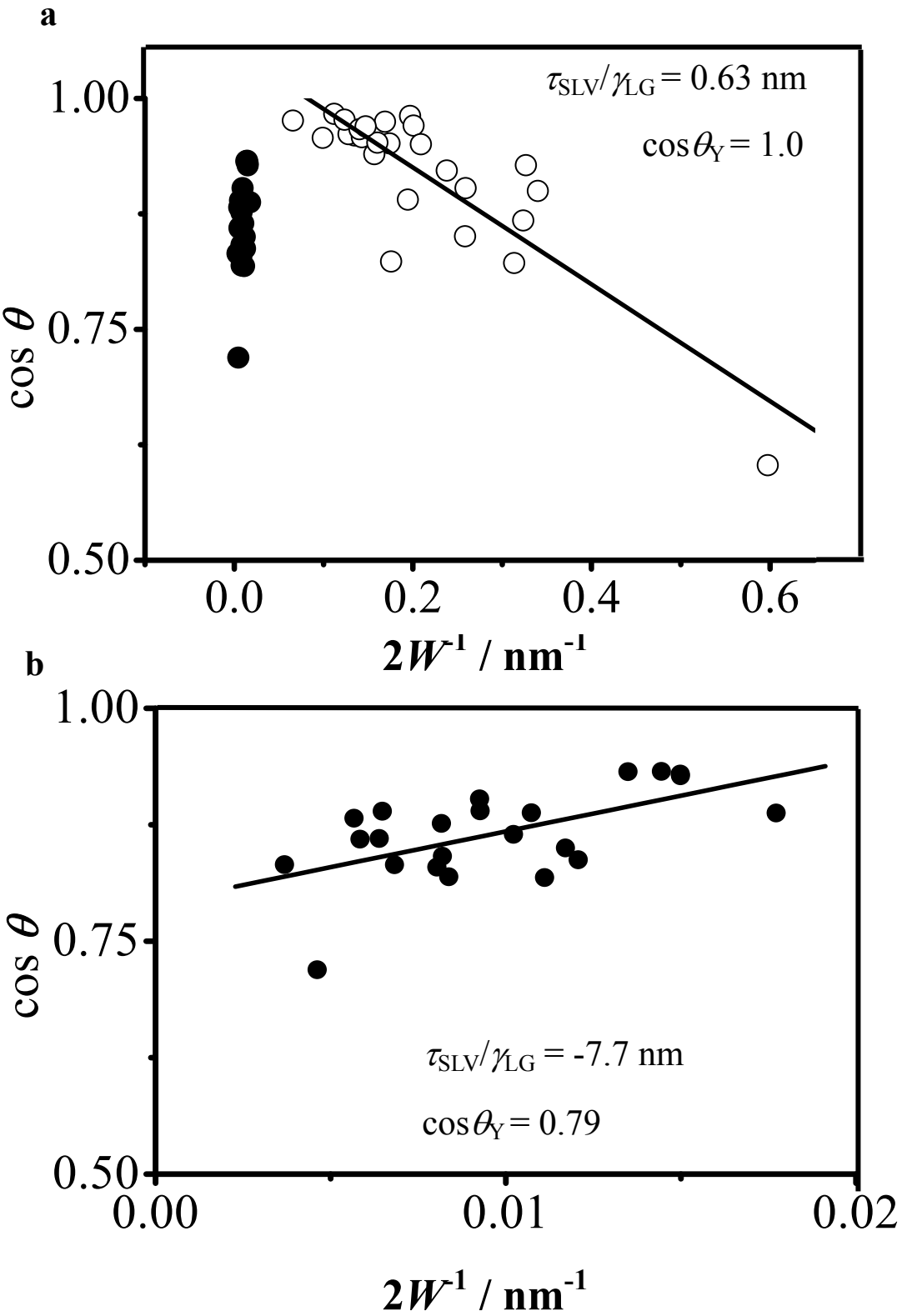
a
τ_{SLV}/γ_{LG} = 0.63 nm
$\cos\theta_Y$ = 1.0
1.00
0.75
0.50
cos θ
0.0
0.2
0.4
0.6
$2W^{-1}$ / nm^{-1}
b
1.00
0.75
0.50
cos θ
τ_{SLV}/γ_{LG} = -7.7 nm
$\cos\theta_Y$ = 0.79
0.00
0.01
0.02
$2W^{-1}$ / nm^{-1}

Table 1

Free energies of the bubbles [a]

W /nm	τ_{SLV} /Jm^{-1}	cos θ_Y	E_S /J	E_L /J	G /J
~ 10 [b]	5.0x10^{-11}	1.0	3.2x10^{-18}	2.4x10^{-18}	5.6x10^{-18}
~ 200 [c]	– 2.0x10^{-10}	0.79	2.7x10^{-16}	–1.3x10^{-16}	1.4x10^{-16}

[a] τ_{SLV} : line energy; E_S : total surface energy/bubble; E_L: total line energy/bubble; G, total Gibbs energy/bubble.

[b] Bubbles in water.

[c] Bubbles in ethanol/water (1/4 in volume) solution.